Flow of winter-transformed Pacific water into the Western Arctic

Robert S. Pickart[a],*, Thomas J. Weingartner[b], Lawrence J. Pratt[a],
Sarah Zimmermann[c], Daniel J. Torres[a]

[a]*Woods Hole Oceanographic Institution, Woods Hole, MA 02543, USA*
[b]*University of Alaska, Fairbanks, Alaska, 99775, USA*
[c]*Institute of Ocean Sciences, USA*

Abstract

The dynamics of the flow of dense water through Barrow Canyon is investigated using data from a hydrographic survey in summer 2002. The focus is on the winter-transformed Bering water—the highest volumetric mode of winter water in the Chukchi Sea—which drains northward through the canyon in spring and summer. The transport of this water mass during the time of the survey was 0.2–0.3 Sv. As the layer flowed from the head of the canyon to the mouth, it sank, decelerated, and stretched. Strong cyclonic relative vorticity was generated on the seaward side of the jet, which compensated for the stretching. This adjustment was incomplete, however, in that it did not extend across the entire current, possibly because of internal mixing due to shear instabilities. The resulting vorticity structure of the flow at the canyon mouth was conducive for baroclinic instability and eddy formation. Multiple eddies of winter-transformed Bering water were observed along the Chukchi–Beaufort shelfbreak. Those to the west of Barrow Canyon were in the process of being spawned by the eastward-flowing shelfbreak current emanating from Herald Canyon, while the single eddy observed to the east originated from the Barrow Canyon outflow. It is argued that such an eddy formation is a major source of the ubiquitous cold-core anti-cyclones observed historically throughout the Canada Basin. Implications for the ventilation of the upper halocline of the Western Arctic are discussed.

1. Introduction

Pacific-origin water flows through Bering Strait into the Chukchi Sea as a result of the large-scale sea-level difference between the Arctic and Pacific (Coachman et al., 1975). While the mean volume

flux of 0.8 Sv is well-documented (Roach et al., 1995), north of the strait the exact pathways by which this water reaches the edge of the Chukchi shelf are still uncertain. One route is the Alaskan Coastal Current in the Eastern Chukchi Sea (Paquette and Bourke, 1974; Mountain, 1974), while another branch extends to the west through Hope Valley (Weingartner et al., 1998). Recently a third branch has been postulated in the central

---

*Corresponding author.

E-mail address: rpickart@whoi.edu (R.S. Pickart).

Chukchi, through the gap between Herald and Hanna Shoals (Weingartner et al., 2005, see Fig. 1). However, recent modeling results suggest that, to a large degree, the northward-flowing water fans out across the entire Chukchi shelf, with little tendency toward forming distinct branches (Winsor and Chapman, 2004). One thing is certain, however, the two major canyons that cut into the Chukchi shelfbreak—Herald Canyon in the west, and Barrow Canyon in the east—play an important role in the channeling of Pacific-origin water toward the open Arctic.

Strong, persistent northward flow has been observed in both Herald and Barrow Canyon (Aagaard and Roach, 1990; Woodgate et al., 2005), although relatively little is known about the circulation near Herald Canyon. This is largely because it is located in Russian territorial waters, which has limited the accessibility of this region. Barrow Canyon, on the other hand, has been the subject of numerous field programs over the years. Early studies documented the seasonality of the northward flow through this canyon. In summertime the buoyant Alaskan Coastal Current carries warm, fresh Bering summertime water into the canyon as a surface-intensified jet (Paquette and Bourke, 1974; Mountain et al., 1976; Munchow and Carmack, 1997). In fall and winter the winds intensify out of the northeast (Furey, 1996), which tends to retard the flow, or block it altogether (Weingartner et al., 1998). During this period, cooling and ice formation over the Chukchi Sea form various classes of winter waters. These have been given a variety of names by different investigators, but in general there are two main classes that we will refer to as winter-transformed Bering water, and hypersaline water. The former is the largest volumetric mode on the Chukchi shelf (see Aagaard and Roach, 1990; Weingartner et al., 1998), with salinities between 32.5 and 33.5 and potential temperatures between -1.4 and $-1.8\,^{\circ}\mathrm{C}$.[1] The latter is the result of enhanced brine-enrichment due to coastal polynyas that form adjacent to the Alaskan Coast (Cavalieri and Martin, 1994; Winsor and Chapman, 2002), with salinities $\geqslant 34.0$ and potential temperatures near the freezing point (see Weingartner et al., 1998). The winter-transformed

Bering water ventilates primarily the upper halocline (see Pickart, 2004), while the hypersaline water is dense enough to ventilate the lower halocline (Weingartner et al., 1998).

In springtime, after the northeasterly winds subside, the recently formed dense water flows through Barrow Canyon as a subsurface current. This flow lasts for several months (Mountain et al., 1976), and can even persist beneath the buoyant Alaskan Coastal Current during the late summer (Paquette and Bourke, 1974; Munchow and Carmack, 1997). It is primarily composed of the winter-transformed Bering water. Northward flow of hypersaline water through Barrow Canyon appears to be relatively rare (Garrison and Becker, 1976; Aagaard and Roach, 1990; Munchow and Carmack, 1997), although plumes of it have been observed (Weingartner et al., 1998).

Aside from the seasonal transition in Barrow Canyon from dense winter-transformed Bering water to buoyant Alaskan Coastal Current water, the dominant variability in the canyon is due to upwelling events. Warm deep water of Atlantic origin is often transported a fair distance up the canyon during episodic events, typically lasting from several days to a week (Aagaard and Roach, 1990). Several mechanisms have been put forth to explain such events. These include response to variations in the sea level pressure difference between the Chukchi Sea and the Arctic (Mountain et al., 1976; Garrison and Becker, 1976), propagation of large-scale coastally trapped waves (Aagaard and Roach, 1990), forcing by local winds (Mountain, 1974), and non-linear rectification due to variations in the northward flowing waters through Barrow Canyon (Signorini et al., 1997). At times the upwelled Atlantic water can extend far onto the Chukchi shelf (Bourke and Paquette, 1976).

The mean speed of the northward-flowing winter-transformed Bering water through Barrow Canyon is $O(15–20)$ cm/s (Aagaard and Roach, 1990). Instantaneously, however, the flow can be much greater than this. The surface-intensified flow of the Alaskan Coastal Current through the canyon is even stronger, with synoptic measurements as large as 75–100 cm/s (Mountain, 1974; Munchow and Carmack, 1997). To date there have been no long-term measurements of the near-surface water through the canyon (due to ice constraints). Synoptic estimates of volume transport through the canyon vary significantly, and can exceed 1 Sv (Munchow and Carmack, 1997). The partitioning of

---

[1] This encompasses winter Chukchi water (Coachman et al., 1975; Garrison and Becker, 1976; Aagaard and Roach, 1990), Bering Sea winter water (Munchow and Carmack, 1997), and Intermediate Chukchi water (Weingartner et al., 1998).

the transport between the summertime and winter-transformed Bering waters—which can flow through the canyon simultaneously—has yet to be done.

Some aspects of the dynamics of the flow through Barrow Canyon have been addressed previously. Munchow and Carmack (1997) were the first to obtain a high-resolution two-dimensional (2-D) section of the velocity field, using a towed Acoustic Doppler Current Profiler (ADCP). This revealed a strong, deep-reaching jet (carrying Alaskan Coastal Current water in the upper layer and winter-transformed Bering water at depth) in approximate geostrophic balance (see Signorini et al., 1997). However, relative vorticities as strong as $6f$ (where f is the local Coriolis parameter) were measured on the offshore side of the jet. This suggests the likelihood of non-negligible ageostrophic effects, and in fact Signorini et al. (1997) demonstrated that a significant secondary (cross-canyon) circulation exists.

Downstream of Barrow Canyon there is some uncertainty as to the fate of the Pacific-origin water. One notion is that the majority of the water (both light and dense) continues eastward along the shelfbreak/upper-slope of the Beaufort Sea as a boundary current (Mountain, 1974; Chapman, 2000; Pickart, 2004). Another suggestion is that the dense winter water sinks down the canyon and enters the deep basin directly (Garrison and Becker, 1976). Either way, there is suggestion that the flow of both warm and cold water exiting the canyon becomes ''ill-behaved'' and subsequently forms eddies. The southern Canada Basin is populated with small-scale eddies (Manley and Hunkins, 1985; Plueddemann et al., 1999) that contain Pacific-origin shelf water (Muench et al., 2000). The vicinity of Barrow Canyon has been postulated as a source region for some of these eddies. Modeling studies of the flow through the canyon have investigated the spawning of eddies from the Alaskan Coastal Current (D'Asaro, 1988) as well as from the winter-transformed water (Shaw and Chao, 2003; Chao and Shaw, 2003; Cenedese and Whitehead, 2000). Direct observation of this process, however, has yet to occur.

The purpose of the present study is to elucidate further the dynamics of the flow of dense water through Barrow Canyon, with an eye towards understanding why this might lead to eddy formation. We focus on the winter-transformed Bering water, and use data from a hydrographic survey conducted in July–August 2002 to investigate the adjustment of the dense water as it flows down the canyon. We begin with a presentation of the data, followed by a kinematic description of the flow. The potential vorticity dynamics are then investigated to understand the impact of the stretching of the layer as it progresses northward. Several cold-core, anti-cyclonic eddies were observed along the shelfbreak; these are described and related to the flow through the two Chukchi Sea canyons. Finally, the ramifications of such eddies on the ventilation of the Western Arctic halocline are considered.

2. Data and methods

2.1. Hydrographic variables

In July–August, 2002 a hydrographic survey was carried out in the Eastern Chukchi/Western Beaufort Seas, as part of the Western Arctic Shelf–Basin Interactions (SBI) program. SBI is a multi-institutional, interdisciplinary project studying the manner in which the Arctic shelves communicate with and influence the adjacent Canada Basin (see Grebmeier and Harvey, 2005). The hydrographic survey in question was carried out aboard the USCGC Polar Star, during which an array of moorings was also set. (A second SBI cruise on the USCGC Healy occurred at the same time, consisting mostly of biological and chemical measurements; see the articles in this special issue). Fig. 1 shows the station locations, consisting mainly of a set of sections crossing the Chukchi/Beaufort shelf-slope boundary. This survey represents the first time that densely spaced measurements have been carried out across the shelfbreak in the Western Arctic. The station spacing for all sections (excluding the central shelf section) was $\leqslant 5$ km, which is smaller than the Rossby radius of deformation at this latitude (8–10 km).

The instrument package consisted of a Seabird 9$+$ conductivity/temperature/depth (CTD) unit mounted on a 24-position frame with 10-l Niskin bottles. A laboratory calibration of the temperature sensors was done before and after the cruise, and an in situ calibration of the conductivity sensors was carried out during the cruise via bottle salinity measurements. Accuracies were determined to be .001 °C for temperature and .002 for salinity (practical salinity scale). Included on the CTD package was a Wetlabs light scattering sensor to measure turbidity, a Seapoint chlorophyll
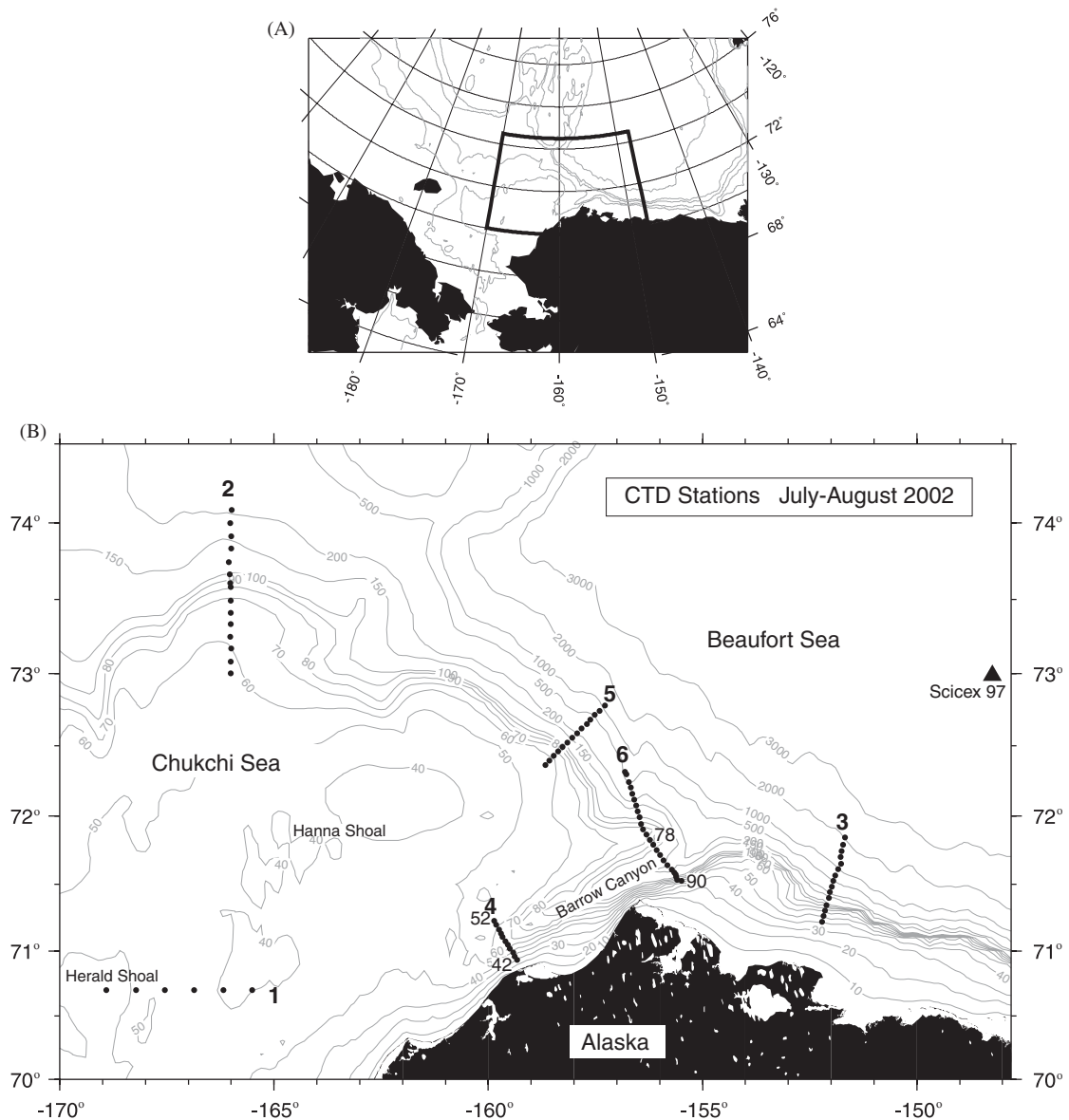
Fig. 1. (A) Study area in the Eastern Chukchi and Western Beaufort Seas. (B) Enlarged view of study area, showing the hydrographic stations occupied by USCGC Polar Star in summer 2002. The survey consisted of six sections. Station numbers are included on the two Barrow Canyon sections: the head of the canyon (stations 42–52) and the mouth of the canyon (stations 78–90). The location of the eddy observed during the 1997 Scicex expedition is indicated by the triangle.

fluorometer, and an RD Instruments dual-work-horse lowered ADCP. Phosphate, nitrate, silicate, and nitrite samples were collected as well, although not at every station due to the fast pace of the survey. Nonetheless, slightly coarser nutrient sections were obtained for all but the last section (no water samples were taken on Section 6 because of a pylon malfunction late in the cruise). Stations were regularly occupied to within 1–2 m above the bottom in order to sample the bottom boundary layer. Standard CTD quality control and pressure averaging were performed to produce 1-db-averaged downcast temperature and salinity profiles, from which potential temperature (θ) and potential density (σ_θ), referenced to the sea surface, were computed.

2.2. Winds

Wind data were obtained using the Polar Star's meteorological sensor suite, mounted 21 m above the sea surface. An average wind vector was computed for each CTD station (while the ship was stopped). Winds throughout the cruise were light; the overall average wind speed was 3.4 ± 1.8 m/s out of the northwest. Hence, at no time during the month-long survey was there an upwelling event in Barrow Canyon (such events are more common during the fall season, corresponding to the passage of Aleutian low-pressure systems).

The two hydrographic sections of particular interest for this study are the lines across the head and mouth of Barrow Canyon (Sections 4 and 6, respectively, Fig. 1). Although these lines were not occupied sequentially, they were separated by only 3 days. This is less than the time for a parcel of dense water to travel the length of Barrow Canyon (order 150 km), so in this regard the two sections can be considered synoptic.[2] Winds during the first crossing (head of the canyon) averaged 3.6 ± 2.7 m/s out of the west/southwest, and during the second crossing (mouth of canyon) the winds averaged 2.9 ± 1.4 m/s out of the northwest.

2.3. Absolute velocity

2.3.1. Estimation of surface velocity

Unfortunately, our lowered-ADCP data are of limited use in Barrow Canyon due to an inappropriate setting in the software for the shallow depth of the canyon (the deep-water lowered-ADCP data are fine). Therefore, we were faced with using geostrophic velocities for our analysis, and, in particular, determining a method of making them absolute. To do this we relied on ship drift.

As it happens, the Polar Star shuts down its propulsion system during the occupation of CTD stations in the presence of ice. In the case of our 2002 survey, the standard procedure was to wait 10–15 min after the screws were disengaged before deploying the CTD, to allow the ship to adjust to

the environmental conditions. The movement of the ship during the cast—i.e. the ship drift—was due to a combination of wind, surface-current, and ice stresses. We used the navigational data to calculate the ship drift during each CTD cast of the two Barrow Canyon crossings. The GPS unit on the Polar Star has a stated accuracy of 5 m. When this is located on the mast of a rolling ship the accuracy for computing ship drift will be less. However, the sea state was flat during both Barrow Canyon crossings (due to the presence of ice and the light winds), so the GPS unit was likely quite stable. To quantify the accuracy, a dock test was conducted after the cruise when the ship was tied to the pier. Over the 90-min period of the test the RMS scatter in the GPS position was ± 3.1 m (this included the effects of small rolls due to the passage of nearby vessels in the harbor). For a 10-min CTD cast (the average duration during the Barrow Canyon stations) this gives a maximum random error of 1 cm/s. Hence the ship-drift calculation is deemed accurate.

The next step is to determine what portion of the drift is due to the surface current. Because the winds were light during the two transects of the canyon, and because during each transect we crossed the swift Alaskan Coastal Current, we assume that the ship drift during each CTD station was due predominantly to the surface current. In other words, we neglect wind drift and ice effects on the movement of the vessel. Ice stresses were likely not a problem because there was a significant amount of open water in the area. This was verified by photographs taken during the cruise, as well as by inspection of the ship's logs. Visual estimates of ice concentration were recorded hourly by the personnel on the bridge, and the average concentration during the two crossings was 0.4 ± 0.2.

As an attempt to quantify the error associated with neglecting the wind drift, we note that the standard rule used by the Coast Guard and other mariners is that vessels drift at roughly 3% of the wind speed and $20°$ to the right of the wind. This can be derived by considering the steady-state force balance on the ship due to the wind and current (J. Trowbridge, pers. comm., 2005). Keep in mind that we waited 10–15 min before estimating the ship drift, during which time the vessel would swing beam into the wind. Under these conditions the drag coefficients in air and water are roughly the same and equal to unity. With this assumption, the difference between the ship drift and surface

---

[2]Munchow and Carmack (1997) found large variations in the flow field within Barrow Canyon on time scales shorter than this. It is worth pointing out, however, that their sections were collected during the fall season when winds are generally stronger. Furthermore, their sections were taken just a few days after an upwelling event occurred in the canyon (Signorini et al., 1997).

current can be written as

$$| \overrightarrow{U_s} - \overrightarrow{U_w} | = \left(\frac{\rho_a A_a}{\rho_w A_w} \right)^{1/2} (| \overrightarrow{U_a} - \overrightarrow{U_s} || \overrightarrow{U_a} |)^{1/2},$$

(1)

where $\overrightarrow{U}$ is velocity, ρ is density, A is the cross-sectional area on which the fluid acts, and the subscripts a, w, and s denote the air, water, and ship. Assuming $A_a = A_w$ and $|\vec{U}_a| \gg ||\vec{U}_s|$, and taking $\rho_a/\rho_w = 10^{-3}$, (1) reduces to $| \overrightarrow{U_s} - \overrightarrow{U_w} | = .03| \overrightarrow{U_a} |$, which is the standard esti-mate noted above. In our case, using a diagram of the ship, A_a/A_w was estimated to be 1.3 (B. Toney, pers. comm., 2005), and since the winds were light we did not implement the assumption that $|\vec{U}_a| \gg ||\vec{U}_s|$. These two factors tend to offset each other, such that the resulting scale factor for the wind remains nearly the same (.031).

Using the measured wind speeds noted above, this results in an error of 10 cm/s for the assumption that the surface current equals the ship drift. This is on the order of 10% based on the observed ship drift of 2 knots in the Alaskan Coastal Current. The error, however, is likely smaller than this. Consider that during the first crossing (head of the canyon) the wind was variable over a range of 60° yet the ship drift in the Alaskan Coastal Current stayed constant to within 8° (mean direction = 65 °T). Then, despite the fact that the wind shifted 55° to the right prior to the second crossing (mouth of the canyon), the ship drift direction remained the same (within 3°). In fact, the predicted wind drift for the second crossing was nearly perpendicular to the observed ship drift. Finally, there was no station-to-station correlation between the wind and ship-drift vectors for either crossing.

Therefore, we are confident that the calculated ship drift is an accurate measure of the surface velocity. We note that there is a nice correspondence of the surface flow of the Alaskan Coastal Current, so computed, and its hydrographic front. Also, the consistency of the volume transport between the two transects (see below) gives us confidence that our method of referencing the geostrophic velocities is sound.

2.3.2. Referencing the geostrophic velocity

To compute the absolute geostrophic velocities we first interpolated the temperature and salinity sections onto a regular grid using a Laplacian-spline objective interpolator. The grid spacing was 1 or 2 km in the horizontal and 5 m in the vertical (note that the CTD station spacing was approximately 2.5 km within the jet). Geostrophic velocities were computed on this grid (using the same objective routine to extrapolate into the bottom triangles), then the component of the surface current normal to the hydrographic section was used to reference the velocities. We define x, u as the distance, velocity normal to the section (positive northeastward), and y, v as the distance, velocity along the section (positive offshore). For the section across the mouth of the canyon, the velocity calculation revealed strong northward flow in the upper layer (the Alaskan Coastal Current), and alternating bands of northward and southward flow at depth (not shown). Such bands of alternating flow are remi-niscent of topographic Rossby waves propagating along a sloping bottom, such as those commonly observed beneath Gulf Stream north of Cape Hatteras (Johns and Watts, 1986; Pickart and Smethie, 1993). Signorini et al. (1997) found wave-like features (both topographic Rossby waves and Kelvin waves) in their model of the flow through Barrow Canyon.

For the purpose of this study we are interested in the seasonal flow of dense water through the canyon, so we applied a filtering technique to remove the high-wavenumber signal from the velocity sections. The technique is similar to that employed by Pickart and Smethie (1993) to remove the topographic wave signal from sections across the Deep Western Boundary Current near Cape Hatteras. Since such waves are bottom-trapped, it makes sense to consider them in a topographic framework. With this in mind we applied a spatial low-pass filter to our gridded velocity data, where the filter is implemented not along lines of constant depth, but along lines of constant height above the bottom (every 5 m). A filter width of 35 km was chosen, which was effective in removing much of the variance of the deep wave signal. The resulting low-passed velocity field was smoothed once more using a 2-D Laplacian filter (to remove noise in the upper portion of the Alaskan Coastal Current, where the bottom-following low-pass filter was less effective). The final filtered absolute geostrophic velocity at the mouth of the Canyon is shown in Fig. 2, along with the high-passed signal that was removed. It reveals a well-behaved, deep-reaching jet flowing northward through the canyon.

The velocity section across the head of the canyon did not show as much spatial variability (for
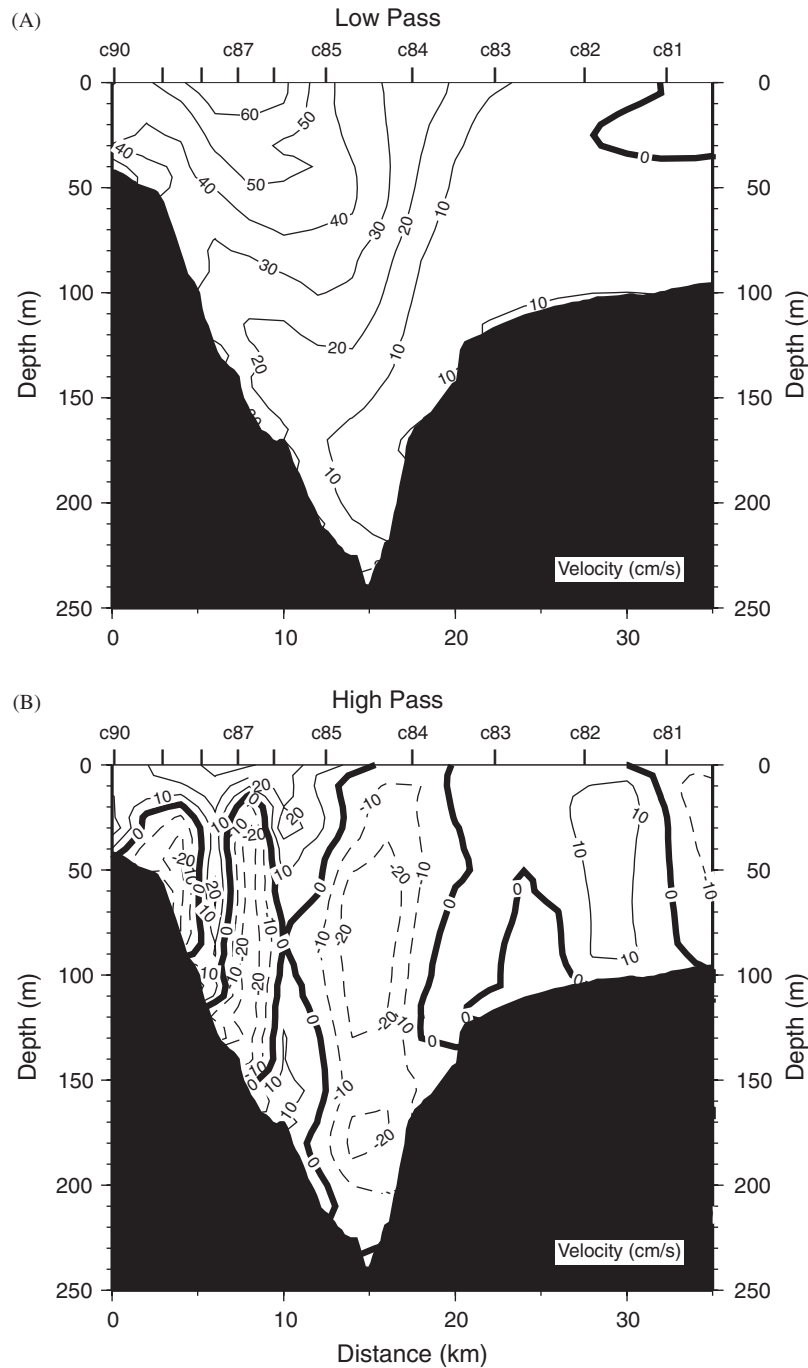
Fig. 2. (A) Filtered absolute geostrophic velocity (cm/s) at the mouth of Barrow Canyon (see text for a description of the filtering technique). Positive velocities (solid contours) are out of the canyon, negative velocities (dashed contours) are into the canyon. (B) High-passed residual velocity (same sign convention for positive and negative velocities).

instance, no flow reversals), but to be consistent with the northern section we applied the same filtering procedure. Since tides are weak in Barrow

Canyon (2–3 cm/s, Danielson, 1996), their contribution is assumed negligible compared to the Alaskan Coastal Current.
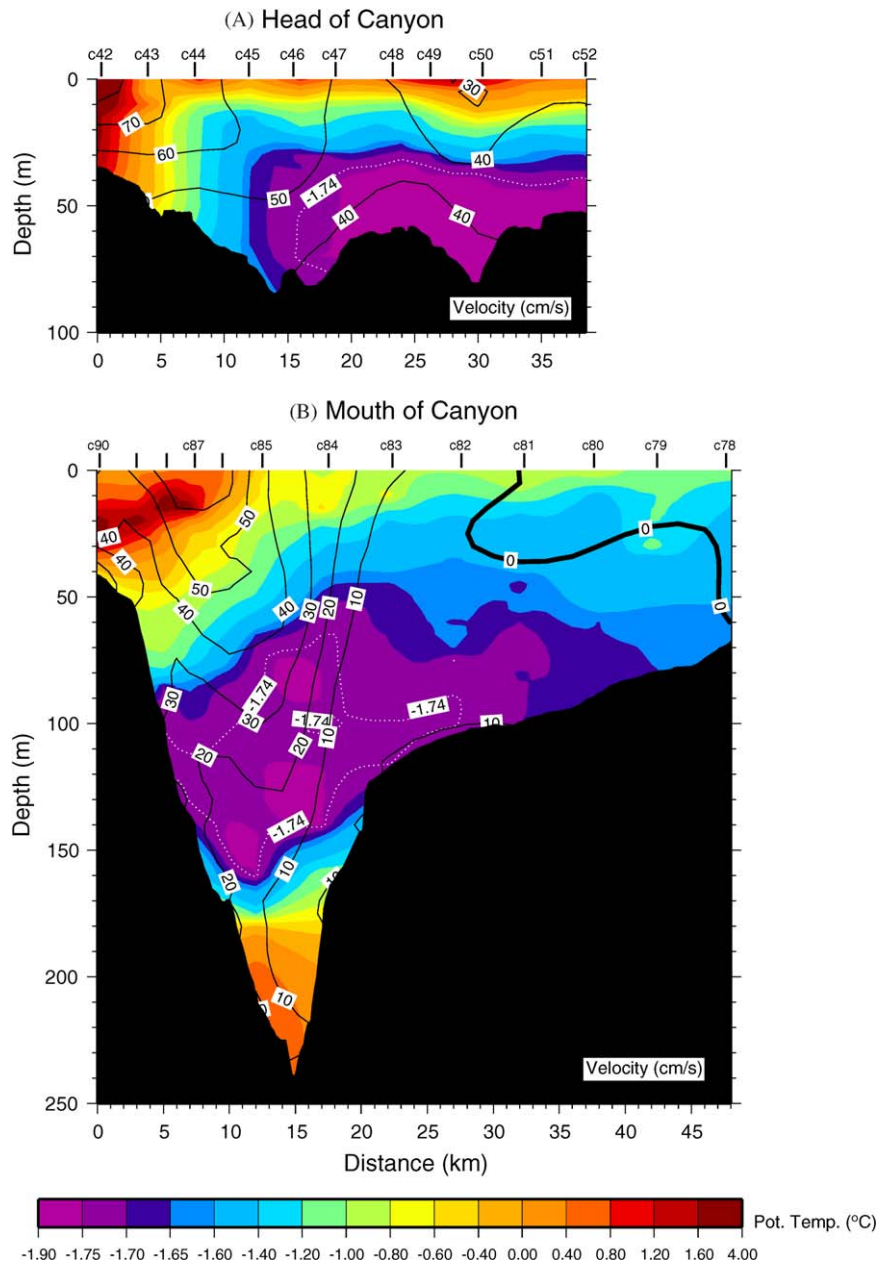
Fig. 3. Vertical sections of filtered velocity (contours, cm/s) overlaid on potential temperature (color, °C). The white dashed line is the −1.74 °C isotherm. (A) Head of Barrow Canyon and (B) mouth of Barrow Canyon.

3. Kinematics and hydrographic properties

The two absolute geostrophic velocity sections are shown in Fig. 3, overlaid on potential temperature. At the head of the canyon (Fig. 3A) one sees the Alaskan Coastal Current flowing northward at > 80 cm/s, advecting warm Bering summertime water > 3.5 °C (the section does not extend far

enough onshore to capture the entire current). The bottom boundary layer in the current is roughly 40 m thick, as seen by the vertically uniform temperature and potential density (Fig. 4A). The temperature color bar used throughout the paper was chosen so that the winter-transformed Bering water corresponds to the magenta shades. Note the uniform layer of winter-transformed water adjacent
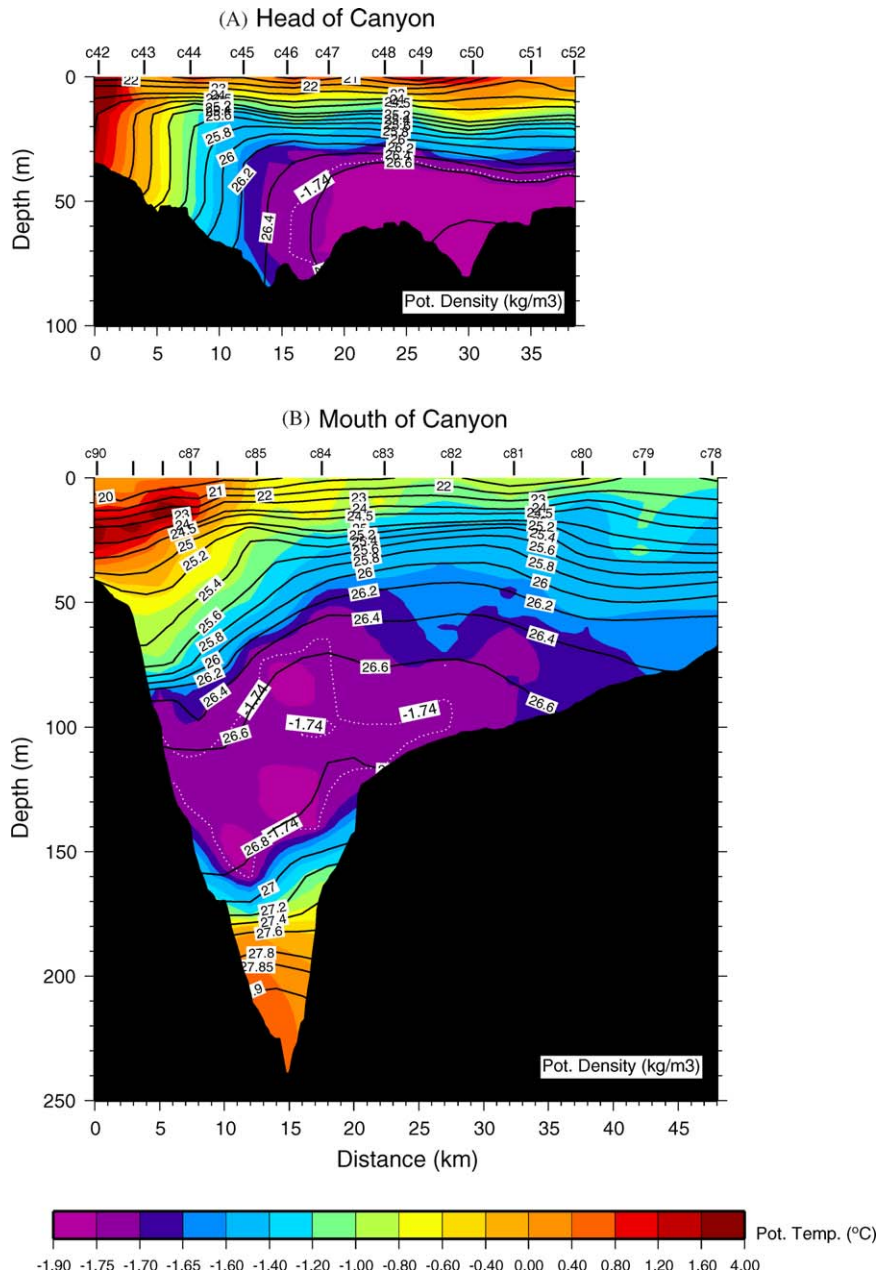
Fig. 4. Vertical sections of potential density (contours, kg/m³) overlaid on potential temperature (color, °C). (A) Head of Barrow Canyon and (B) mouth of Barrow Canyon.

to the Alaskan Coastal Current at the head of the canyon, also flowing northward (Figs. 3A and 4A). We are particularly interested in the adjustment and fate of this dense water as it flows down the canyon. Its origin is likely the central Chukchi shelf; this is consistent with current meter data from the southern flank of Hanna Shoal (Fig. 1) showing a generally steady eastward flow toward the canyon (Weingartner et al., 2005).

At the end of the winter season, this dense water represents a reservoir at the top of Barrow Canyon. It is also a source of high silicate for the Arctic (Fig. 5A), likely due to the re-suspension of nutrients from the bottom sediments on the Chukchi shelf. This is consistent with the elevated turbidity in the lower part of the water column (Fig. 5B). We note that this contradicts the traditional view that the sole source of high-nutrient
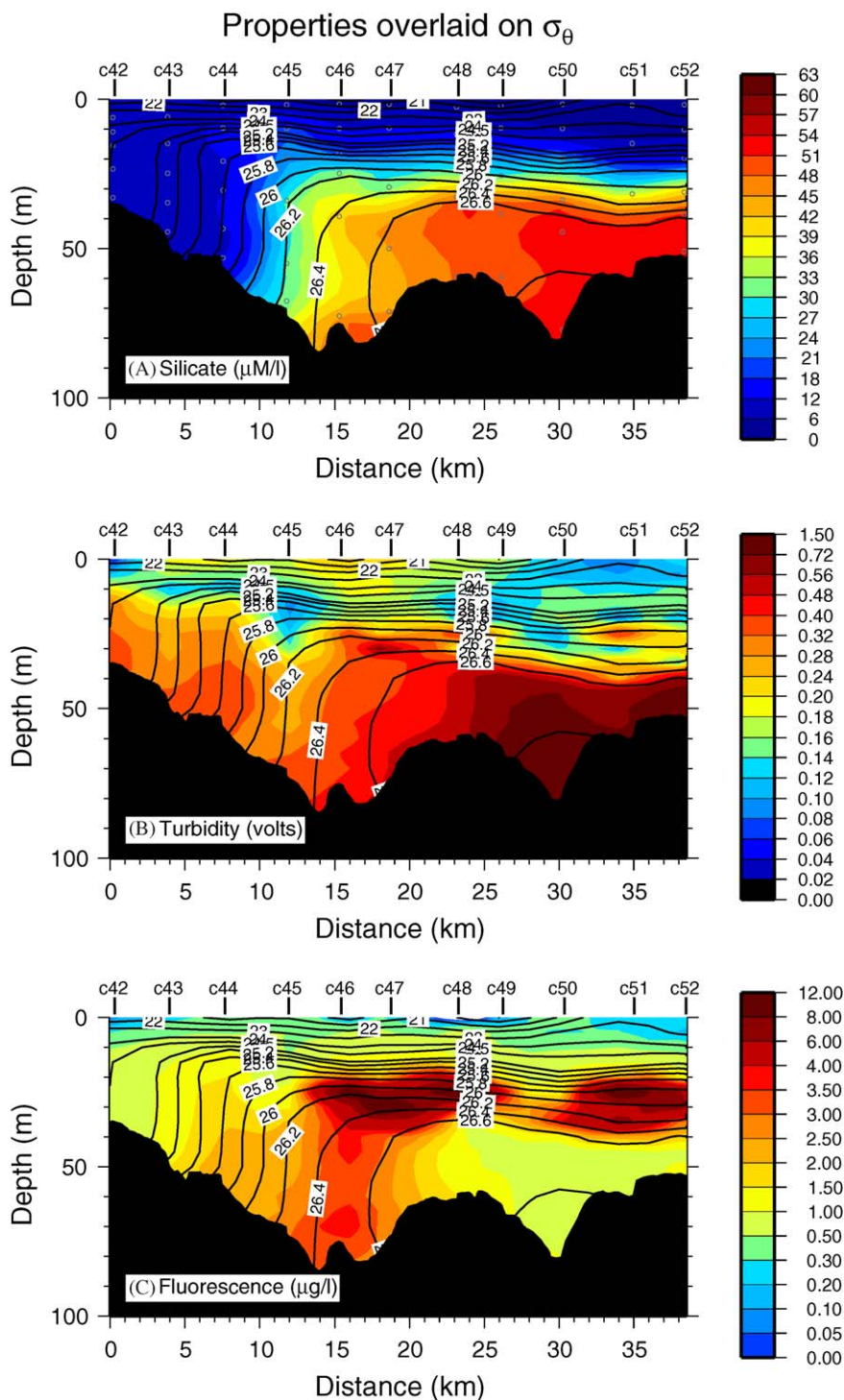
Fig. 5. Vertical sections at the head of Barrow Canyon. The contours are potential density (kg/m^3): (A) Silicate (color, µM/l); Water sample locations are indicated by the circles, (B) turbidity (color, volts) and (C) fluorescence (color, µg/l).

Chukchi shelf water into the Arctic is through Herald Canyon in the west. The fluorescence signal at the head of Barrow Canyon is also intriguing (Fig. 5C), indicating elevated values of chlorophyll on the Chukchi shelf within the main pycnocline (near 25 m) at this time of year. This signal follows

the nutricline, while the surface waters seem to be nitrogen-limited. Near the seaward edge of the Alaskan Coastal Current the high fluorescence extends vertically into the bottom boundary layer, right to the seafloor (near $y = 15$ km). This may be due to a combination of convergence/downwelling in the coastal current as well as the sinking of the phytoplankton mass. It is unlikely that local production is occurring near the bottom, based on measurements conducted in Barrow Canyon during the concurrent SBI cruise aboard the USCGC Healy. The CTD package on the Healy included a PAR sensor, and primary production experiments were carried out. These indicate that the 1% light level extended only to 50 m and that production did not occur deeper than this (Hill and Cota, 2005). Due to such a distribution of fluorescence in the canyon, some of the signal readily diffuses into the layer of winter-transformed Bering water (Fig. 5C). The ramifications of this are discussed later in the paper in the discussion on eddy formation.

The adjustment of the flow from the head of the canyon to its mouth—a distance of roughly 150 km—is striking. At the head of the canyon, the Alaskan Coastal Current and the winter-transformed water flow side by side (Fig. 3A). At the downstream section (Fig. 3B) these two features have re-arranged themselves into a narrow, deep-reaching jet in which the winter-transformed water is now essentially beneath the Alaskan Coastal Current water. (Atlantic-origin water occupies the deepest part of the canyon.) Using an advective speed of 30 cm/s for the dense water and a net vertical displacement of 70 m (within the down-stream jet), this gives a vertical velocity of 12 m/day. Note that the winter-transformed water warms as it sinks. This is likely due to diffusion more than entrainment, since the water occupies roughly the same density class at the two sections, $26.4 < \sigma_\theta < 26.85$, and the volume transport is essentially conserved within this layer. In particular, the transport at the upstream section is 0.29 Sv, while at the downstream section it is 0.24 Sv. In light of the uncertainty noted above in the surface currents used to reference the geostrophic velocities, these transport values are probably indistinguishable. This suggests that an isopycnal framework is appropriate for studying the dynamics of the flow through the canyon. In Figs. 3 and 4 the $-1.74\,^\circ$C isotherm has been contoured (white dashed line), delimiting the coldest winter-transformed water. At the mouth of the canyon (Fig. 3B) the offshore edge

of this water coincides with the offshore edge of the deep jet (the 10 cm/s isotach). Hence, during the adjustment, the coldest water has moved toward the shoreward side of the canyon.

4. Dynamics of adjustment in the Canyon

4.1. Potential vorticity

Using the gridded velocity and hydrographic sections, we computed fields of the potential vorticity. Because of the strongly sloped isopycnals at both the head and the mouth of the canyon (for instance in the bottom boundary layer of the Alaskan Coastal Current at the head of the canyon), it was necessary to consider the Ertel potential vorticity,

$$\Pi = \frac{-f}{\rho_0} \frac{\partial \sigma_\theta}{\partial z} + \frac{1}{\rho_0} \frac{\partial u}{\partial y} \frac{\partial \sigma_\theta}{\partial z} - \frac{g}{\rho_0^2 f} \left(\frac{\partial \sigma_\theta}{\partial y} \right)^2, \qquad (2)$$

where f is the (constant) Coriolis parameter ($1.38 \times 10^{-4}\,\mathrm{s}^{-1}$), ρ_0 is the reference density ($1.027 \times 10^3\,\mathrm{kg\,m}^{-3}$), and g is the gravitational acceleration. The first two terms in (2) are the planetary stretching and the relative vorticity, which are present in a quasi-geostrophic framework (note that since $v_x \ll u_y$ in Barrow Canyon, the relative vorticity is due primarily to the cross-canyon gradient of the along-canyon velocity). The third term in (2) is the tilting vorticity, a non-quasi-geostrophic term that arises because of the strong cross-canyon gradients in density. Hall (1994) presents a thorough derivation and discussion of the Ertel potential vorticity for a similar case in the Gulf Stream.

In weak or large-scale flows, the stretching term in (2) is generally dominant. However, as seen in Figs. 6 and 7, both the relative vorticity and the stretching vorticity were significant in parts of Barrow Canyon during our hydrographic survey. In particular, the deep-reaching jet at the mouth of the canyon is characterized by significant relative vorticity of both signs (Fig. 6B): cyclonic vorticity on the seaward side of the jet, strongest at mid-depth; and anti-cyclonic vorticity on the shoreward side, strongest near the surface in the Alaskan Coastal Current. In both instances values exceeded $0.5f$, which is consistent with the values Munchow and Carmack (1997) observed previously in Barrow Canyon. At the head of the canyon relative vorticities were generally weak (Fig. 6A).
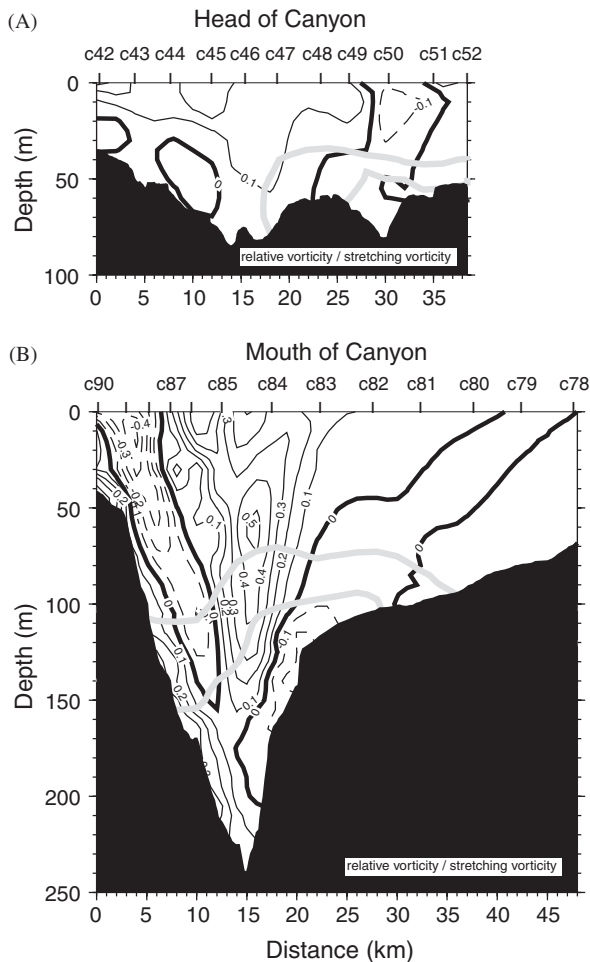
Fig. 6. Vertical sections of the ratio of relative vorticity to stretching vorticity (see Eq. (2)). Solid contours are cyclonic vorticity, dashed contours are anti-cyclonic. The thick gray lines show the density layer chosen for the vorticity analysis ($\sigma_\theta = 26.6 - 26.75$). (A) Head of Barrow Canyon and (B) mouth of Barrow Canyon.
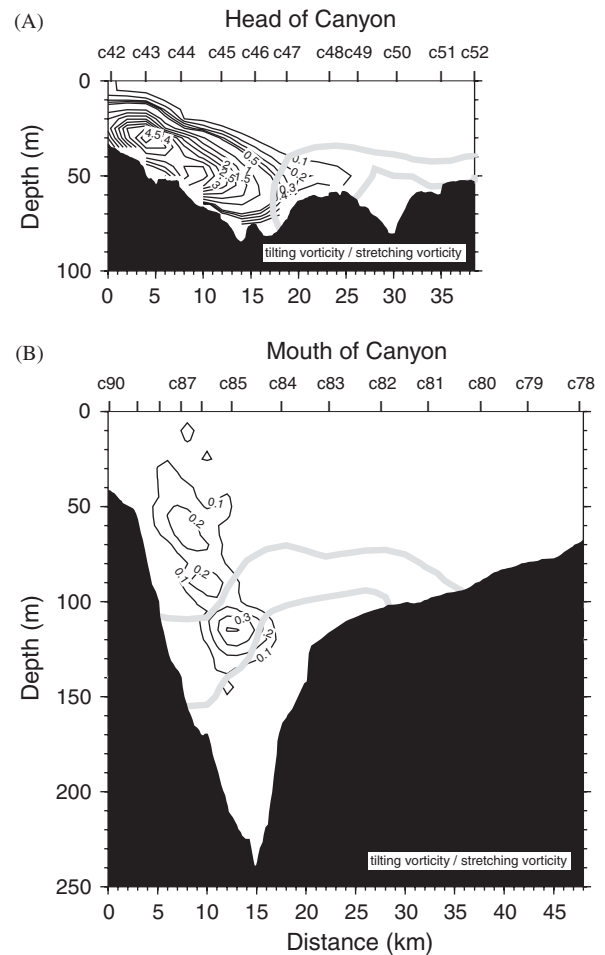

Fig. 7. Vertical sections of the ratio of tilting vorticity to stretching vorticity. The thick gray lines are as in Fig. 6. (A) Head of Barrow Canyon and (B) mouth of Barrow Canyon.

By contrast, the tilting vorticity is the dominant term in the bottom boundary layer of the Alaskan Coastal Current at the head of Barrow Canyon (Fig. 7A), with values 3–4 times greater than the stretching vorticity. Even at the mouth of the canyon the tilting term can be significant, with values 40% as strong as the stretching vorticity in the center of the deep-reaching jet (Fig. 7B). For the purposes of this study we are interested in the evolution of the dense winter-transformed Bering water as it flows down the canyon. Accordingly, we considered the potential vorticity balance within the density layer 26.6–26.75. This layer does not quite encompass the entire winter-transformed water

mass (Fig. 4), but this was done to avoid "edge effects" (near the bounding water masses) when computing the vorticity terms. The upper and lower bounds of the density layer are shown in Figs. 6 and 7. We confine ourselves to the broad part of the layer at the head of the canyon ($18 \, \text{km} < y < 28 \, \text{km}$, where the layer is bounded below by the topography), and the onshore part of the layer at the mouth of the canyon ($y < 25 \, \text{km}$). The transport is virtually identical in these two regions, so we are indeed considering the part of the flow that undergoes the adjustment.

As seen in Figs. 6A and 7A, both the relative vorticity and tilting vorticity are small in the winter-transformed layer at the head of Barrow Canyon (10–15% of the stretching vorticity). However, during the adjustment through the canyon both of
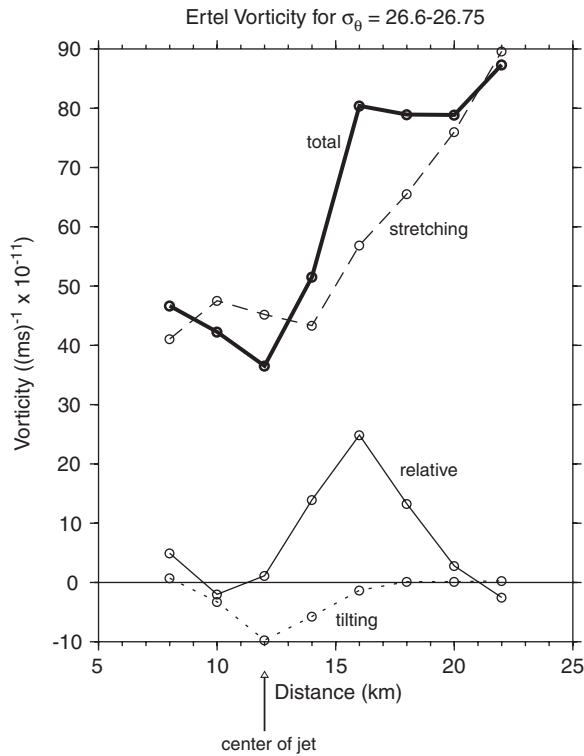
Fig. 8. Terms of the Ertel vorticity at the mouth of Barrow Canyon, averaged over the density layer $\sigma_\theta = 26.6-26.75$ (see Eq. (2)). The center of the deep jet is marked by the arrow.

Fig. 9. Terms of the shallow-water vorticity at the mouth of Barrow Canyon, averaged over the density layer $\sigma_\theta = 26.6-26.75$ (see Eq. (3)). The center of the deep jet is marked by the arrow. The average value of Q at the head of the canyon ($18\,\text{km} < y < 28\,\text{km}$) is shown by the thick dashed line (standard deviation indicated by the bar).

these terms become important (40% as large as the stretching term at the downstream section). The ramifications of this can be seen in Fig. 8, which shows the layer-averaged cross-stream distribution of vorticity at the mouth of the canyon. On the offshore side of the jet the large cyclonic relative vorticity causes Π to deviate substantially from the stretching value, and in the center of the jet the tilting vorticity does the same. Note that the cyclonic side of the jet is broader than the anti-cyclonic side (this is evident in Fig. 6B as well), and that the anti-cyclonic relative vorticity is negligible.

Therefore, from the top of Barrow Canyon to its mouth, the layer of winter-transformed water decelerates, undergoes significant stretching (see Fig. 4), and, as a result, generates significant cyclonic relative vorticity. Does the value of relative vorticity so attained make sense? To answer this one needs to compute the analogous layer-averages for the section across the head of Barrow Canyon. Unfortunately however, the sharp pycnocline at the top of the layer in this region makes this calculation problematic. In particular, the large value of $\partial\sigma_\theta/\partial z$
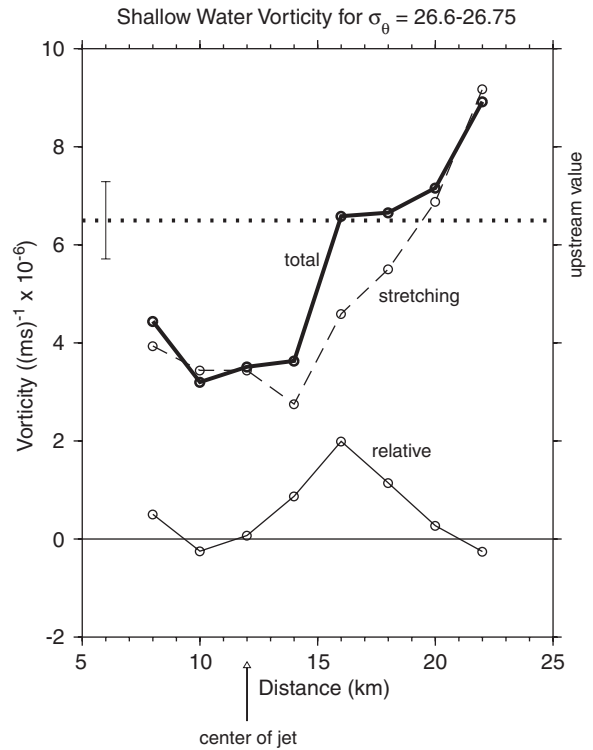
near the upper edge dominates the layer average (and choosing a thin enough layer to avoid this makes the result too uncertain). Note, however, that the tilting term is not relevant in this discussion, since it is negligible where the cyclonic vorticity is large (Fig. 8). Hence, we can answer the above question by considering the shallow water potential vorticity,

$$Q = \frac{(f + \zeta)}{h}, \tag{3}$$

where $\zeta = u_{y,}$ and h is the layer thickness. This quantity is straightforward to calculate from the gridded sections, and it is not subject to the edge effects encountered above. At the head of Barrow Canyon Q is dominated by f/h, with an average value of $6.5 \pm 0.8\,(\text{ms})^{-1} \times 10^{-6}$. Fig. 9 shows the cross-stream distribution of Q, and its two constituents, at the mouth of the canyon. One sees that the stretching and the relative vorticity distributions

are essentially the same as for the Ertel formulation.[3] However, it is now clear that the cyclonic vorticity which is generated during the adjustment compensates exactly the stretching of the water column, so as to conserve the upstream value of Q. This in turn causes a plateau in Q (and Π) to develop within the seaward part of the jet (Figs. 8 and 9). The question now is, why doesn't this potential vorticity adjustment extend across the entire jet?

4.2. Mixing and hydraulics

One possible explanation for the non-conservation of the potential vorticity on the shoreward side of the jet is that it is due to sidewall friction. The lowered-ADCP velocity data from multiple SBI cruises provide the opportunity to investigate the high-wavenumber signal and the importance of mixing. This will hopefully shed light on the issue at hand, but at present the analysis is not far enough along to be definitive. We can, however, do a simple scale analysis to see if lateral mixing is a possibility. The length over which frictional effects extend is given by the Munk boundary layer thickness, $\delta_{\mathrm{m}} = (A_H \beta_0)^{1/3}$, where A_H is the lateral viscosity and $\beta_0 = sf/H$ is topographic beta. Using a bottom slope s of .012 for Barrow Canyon and a layer thickness H of 50 m, this gives $\beta_0 = 3 \times 10^{-8} (\mathrm{ms})^{-1}$. In order for δ_{m} to extend into the shoreward part of the jet (order 5 km), this would require A_H to be of the order $10^3 \mathrm{m^2 s^{-1}}$, which is not unreasonable (Pedlosky, 1979).

A second possible reason why Π may not be conserved onshore is due to internal mixing resulting from shear instabilities. For this to be the case, the vertical shear in velocity must generally be strong enough to make the Richardson number $Ri = (N/u_z)^2$ less than unity, where u is the downstream velocity and N is the buoyancy frequency. Approximating u_z by u/H where H is the vertical length scale, yields a bulk form of the Richardson number, $Ri = 1/F^2$, where $F = u/NH$ is an internal Froude number. Choosing $H = 50$ m as above, we used the gridded sections of N and u to compute a vertical section of F, which is shown in Fig. 10. For the density layer in question, the combination of strongly sloped isopycnals in the center of the jet (which translates to weak vertical stratification) and

---

[3]Note that the magnitude of Π and Q differ by a factor of $\Delta\rho/\rho_0$, which for the density layer in question is $O(10^{-4})$.
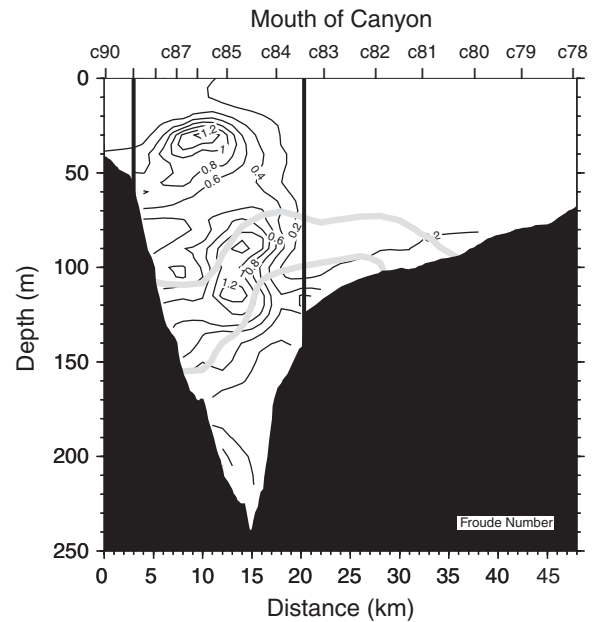

Fig. 10. Vertical section of Froude number (see text for definition) at the mouth of Barrow Canyon. The thick gray lines are as in Fig. 6. The vertical black lines denote the artificial edges of the canyon used to solve Eq. (4).

the strong flow, leads to a sharp enhancement of the Froude number (values >1). Note that F attains these large values (Ri falls below unity) at the location where the conservation of potential vorticity breaks down, near $y = 16$ km (Fig. 8).

The fact that the internal Froude number gets as large as unity suggests that the deep-reaching jet may be supercritical and that hydraulic processes may be important in Barrow Canyon. A similar situation has been shown to exist in the Faroe Bank channel of the North Atlantic, where the flow is believed to be hydraulically controlled (Borenas and Lundberg, 1988). If a subcritical-to-supercritical transition takes place in Barrow Canyon, a hydraulic jump or strong lee wave might result. Either of these could be responsible for altering the potential vorticity of the dense winter-transformed water flowing down the canyon. Hydraulic control in the canyon could have strong implications for the upstream dynamics in the Chukchi Sea, since it would imply limits on how rapidly fluid could be drained from the shelf. The limiting factor would involve the width of the canyon.

A thorough hydraulic analysis is beyond the scope of our data. However, we can get a better indication of whether or not hydraulic effects are

present by calculating the long, internal gravity wave speeds of the system. Hydraulic processes can act when the flow is strong enough to arrest upstream propagation of long waves (i.e. it is supercritical). We are therefore interested in the propagation speeds of, say, the first few internal modes. In order to determine these speeds properly one must take the effects of stratification and vertical shear into account. Speeds for given profiles of $N(z)$ and $u(z)$ are calculated by solving the Taylor–Goldstein equation. Recently Pratt et al. (2000) extended this equation to account for non-uniformities in the cross-sectional topography of the channel. The method of solution assumes, however, that the velocity and density are uniform across the channel. Following Pratt et al. (2000), we divided the water column into 15 discrete layers and computed canyon-averaged profiles of buoyancy, frequency and velocity from our gridded fields. To compute these averages, the sides of the canyon were artificially extended to the surface as depicted in Fig. 10. The governing equation is

$$(u - c) \frac{d^2 w}{dz^2} + \left[\frac{N^2}{u - c} - \frac{d^2 u}{dz^2} \right] w + \frac{d}{dz}[(u - c)Tw] = 0, \tag{4}$$

where w is the amplitude of the vertical velocity of the internal gravity wave, c is the wave speed, u is the background jet velocity, and $T = b^{-1} \, db/dz$, where $b(z)$ is the width of the canyon as a function of depth. The boundary conditions are that w vanishes at the surface and at the deepest depth, $z = D$ of the channel:

$$w(0) = w(D) = 0. \tag{5}$$

The eigenvalues of (4) and (5) are the discrete dynamical, long-wave modes of the flow. When the Richardson number is everywhere greater than $\frac{1}{4}$ there are an infinite number of modes. Each mode is associated with two waves: one that propagates with the flow (positive), and the other that usually propagates counter to the flow towards the Chukchi Sea (negative). We are primarily interested in the latter. If the speed of this wave is in fact positive (indicating propagation out of the Chukchi Sea) or negative but of a magnitude much less than the speed of its sister mode, then hydraulic behavior is strongly indicated.

The solution to (4) and (5) for the observed deep jet in Barrow Canyon is shown in Fig. 11. Only the first three dynamical modes are included. The top panel shows the vertical structure of the upstream
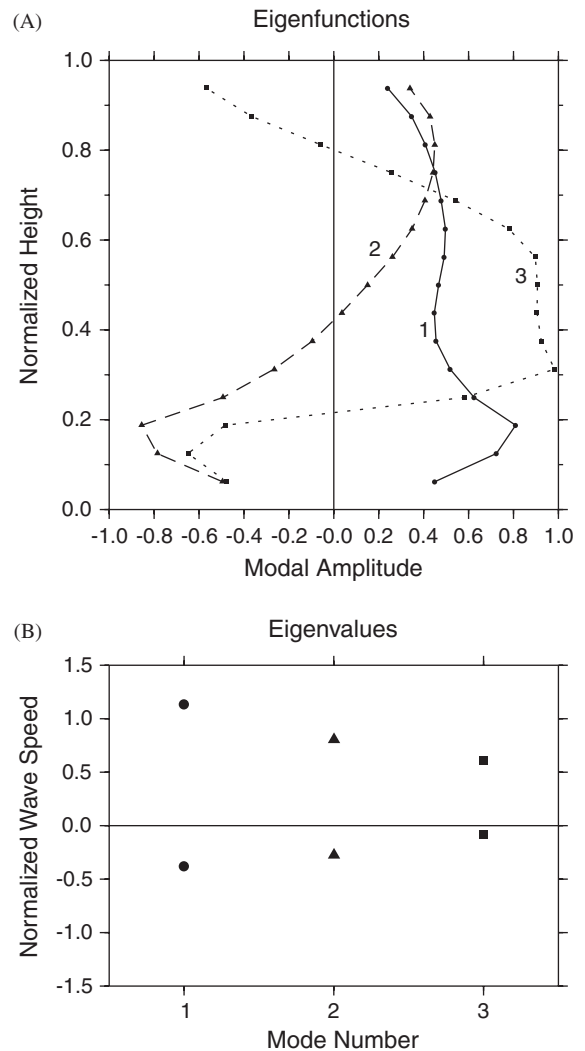
Fig. 11. Solution to the modified Taylor-Goldstein equation for the mouth of Barrow Canyon: (A) vertical structure of the first three dynamical modes and (B) wave speeds of the first three modes (symbols the same as in (A)).

propagating mode (which is similar in character to the downstream propagating mode), and the bottom panel shows the wave speeds of each modal pair. A mode is supercritical if both of these wave speeds are positive (i.e. propagating towards the Arctic). While none of the Barrow Canyon modes are strictly supercritical, the results nonetheless suggest that the flow may be hydraulic in character. This is due to the strong asymmetry in the wave speeds of the modes; namely, that the negative phase speeds approach zero with higher mode number. For mode 3, the upstream propagating wave is essentially stationary. This is significant

because it is this mode which is the most relevant for the Barrow Canyon dense water case. To wit, the winter-transformed Bering water is flowing out at mid-depth (below the Alaskan Coastal Current water and above the Atlantic water), which is consistent with the vertical structure of mode 3 (Fig. 11A). We conclude that hydraulic control may be active in Barrow Canyon, and that small-scale mixing may contribute to the non-conservation of potential vorticity during the adjustment of the dense water as it flows down the canyon. Clearly, more detailed study of the hydraulics is required. For instance, an analysis using directly measured (non-smoothed) velocity, over a period of several days, would be enlightening.

5. Shelfbreak eddies

5.1. Formation mechanisms

It is well documented that the Canada Basin contains a large number of ubiquitous eddies (Manley and Hunkins, 1985) that are filled with Pacific-origin water (Muench et al., 2000). They are typically 15–25 km in diameter, and are located predominantly in the depth range 50–150 m (Manley and Hunkins, 1985; Krishfield and Plueddemann, 2002). To date, their place of origin, as well as the manner in which they are formed, have not been determined. However, the Chukchi Sea is clearly the ultimate source of water in these features. Both warm-core and cold-core eddies have been observed, and most spin anti-cyclonically.

Various mechanisms have been put forth to explain the generation of the eddies. The explanations fall into two general classes: current-topography interactions, and hydrodynamic instability. Most of the explanations in the former class apply explicitly to Barrow Canyon. For instance, D'Asaro (1988) proposed that frictional torque, generated when the Alaskan Coastal Current flows against the side of Barrow Canyon, leads to eddy formation. However, it is unlikely that such strong anti-cyclonic vorticity exists in the canyon (see Fig. 6, as well as Munchow and Carmack, 1997). More relevant to the discussion at hand, Cenedese and Whitehead (2000) investigated dense water flowing through Barrow Canyon in a laboratory setting. They found that the sharp change in coastline at the canyon mouth, in conjunction with the steepening of the continental slope, led to the generation of anti-cyclones. Most recently, Shaw and Chao (2003)

and Chao and Shaw (2003) did a numerical study of eddy formation due to dense water flowing down an Arctic canyon, with application to Barrow Canyon. Anti-cyclones were spawned by the sinking current, and this process was enhanced by the presence of ambient flow farther offshore.

Our vorticity analysis in the previous section does not explicitly support nor contradict the Cenedese and Whitehead (2000) hypothesis, or the mechanisms put forth by Shaw and Chao (2003) and Chao and Shaw (2003). We note, however, that the orientation of the continental slope does not change between our two hydrographic lines (Sections 4 and 6, Fig. 1), so the change in curvature investigated by Cenedese and Whitehead (2000) does not apply to our case. Furthermore, the westward-flowing Beaufort Gyre as well as Aagaard's (1984) eastward-flowing Beaufort Undercurrent—the two ambient flows investigated by Shaw and Chao (2003) and Chao and Shaw (2003)—are located offshore of our downstream hydrographic section.[4] Hence these features also do not apply to the present situation.

Are there any aspects of the potential vorticity adjustment described above that could facilitate eddy formation? Two factors are worth mentioning. Note in Fig. 8 that, onshore of the plateau in π, the decrease in relative vorticity along with the generation of tilting vorticity cause a precipitous drop in the value of the potential vorticity. This not only produces a sharp front, but creates an abrupt change in sign of $d\Pi/dy$ at the center of the jet. This change in sign is a necessary condition for baroclinic instability of the current (Pedlosky, 1979), which is conducive for eddy formation. Furthermore, the potential vorticity front in Fig. 8 is analogous to that found in the Gulf Stream (Hall, 1985). Pratt and Stern (1986) have demonstrated that such a feature can lead to eddy formation via non-linear steepening of the path of the current at finite amplitude. Hence, our results suggest that an initial disturbance arising from baroclinic instability of the flow of dense water through Barrow Canyon could quickly become enhanced and pinch off an anti-cyclone (see Fig. 22 in Pratt and Stern, 1986).

The second general type of eddy formation does not involve anomalous topography such as a canyon, but instead is due to "generic" hydrodynamic instability of the flow. Manley and Hunkins (1985) proposed that eddies would likely be formed

---

[4]The concept of a deep-reaching Beaufort Undercurrent has recently been called into question, see Pickart (2004).

via baroclinic instability of the boundary current along the southern Canada Basin. They identified the Alaskan Coastal Current (downstream of Barrow Canyon) as a possible source of the observed warm-core eddies. Instability of such a surface-intensified flow leads to eddy formation in other areas of the world ocean, such as the shelfbreak jet of the Middle Atlantic Bight (Garvine et al., 1988). However, in order for the Alaskan Coastal Current to be source of the Canada Basin eddies described above, this would require a mechanism for transforming the eddies into subsurface features after they are formed. Manley and Hunkins (1985) hypothesized that friction exerted by the pack ice in the central basin might accomplish this, and Ou and Gordon (1986) modeled this process numerically. However, while the Alaskan Coastal Current does indeed form eddies, they are likely not the subsurface features observed by Manley and Hunkins (1985) in the interior (see below).

A second flavor of baroclinic instability in the southern Canada Basin boundary current has been suggested recently by Pickart (2004). Using historical data from the Alaskan Beaufort Sea, he showed that when the shelfbreak jet advects winter-transformed Bering water in late spring and summer, its potential vorticity structure is conducive for baroclinic instability (in a manner distinct from that described above for Barrow Canyon). It was speculated that the Canada Basin cold-core anti-cyclonic eddies could be formed from this seasonal current. We now verify this, using our hydrographic data from the shelfedge.

5.2. Observed anti-cyclones

As seen in Fig. 1, our survey included four hydrographic sections across the shelfbreak and upper slope (the outer portion of Section 6 constitutes one of the crossings). The sections to the west of Barrow Canyon revealed that winter-transformed Bering water, likely originating from Herald Canyon, flows eastward as a boundary current centered near the shelfbreak—just as it does to the east of Barrow Canyon (Pickart, 2004). Hence, the concept of the "Beaufort shelfbreak jet" put forth by Pickart (2004) should be extended to include the Chukchi shelfbreak as well. Strikingly, at each of our cross-slope sections we observed either an eddy being formed from this boundary current, or a fully detached eddy just offshore of it

(Fig. 12). This represents strong evidence that the shelfbreak jet is a source of the Canada Basin cold-core eddies.

In Fig. 12A, to the west of Barrow Canyon (Section 5 in Fig. 1), the downward-sloping isopycnals near the edge of the shelf correspond to the sub-surface intensified eastward shelfbreak jet. Offshore of this, centered at stations 61 and 64, are two lenses of boundary current water that are likely anti-cyclonic eddies being spawned from the current, in a manner similar to that seen in the numerical studies of Spall (1995) and Bush et al. (1996). We note that since our section is a 2-D snap shot, we could instead have sampled a meander of the current. However, the "pinching" of the cold water at station 59 suggests that eddy formation was imminent.[5] One sees that these features are carrying with them high sediment loads (Fig. 12A) as well as elevated values of fluorescence and silicate (not shown). A similar pinching was observed as well at the other two sections west of Barrow Canyon, indicating that this process is very active, and, presumably very efficient at transporting properties from the shelf to the basin.

The section to the east of Barrow Canyon also shows an anti-cyclonic cold-core eddy filled with winter-transformed Bering water (Fig. 12B). The difference here is that this eddy seems to be fully detached from the boundary current—note the absence of cold boundary current water near the shelfbreak. This could be due to a temporary disruption of the current due to the eddy-formation process, or it might be that the boundary current is starting to "disintegrate" at this location and time (see Pickart, 2004 for a description of the seasonal evolution of the shelfbreak jet). The latter may be more likely. During the cruise we deployed an array of moorings along Section 3, and the first year of data indicated that the winter-transformed Bering water was nearly depleted by August of 2002. Hence our survey sampled the tail end of the previous winter's Chukchi Sea water mass product.

The detached eddy at Section 3 is also characterized by high values of turbidity (Fig. 12B) as well as fluorescence and silicate (not shown). The other interesting feature in Fig. 12B is the lens of warm water in the upper 40 m of the water column seaward of the shelfbreak (stations 30–33 in Fig. 12B). This is a surface-intensified anti-cyclonic

---

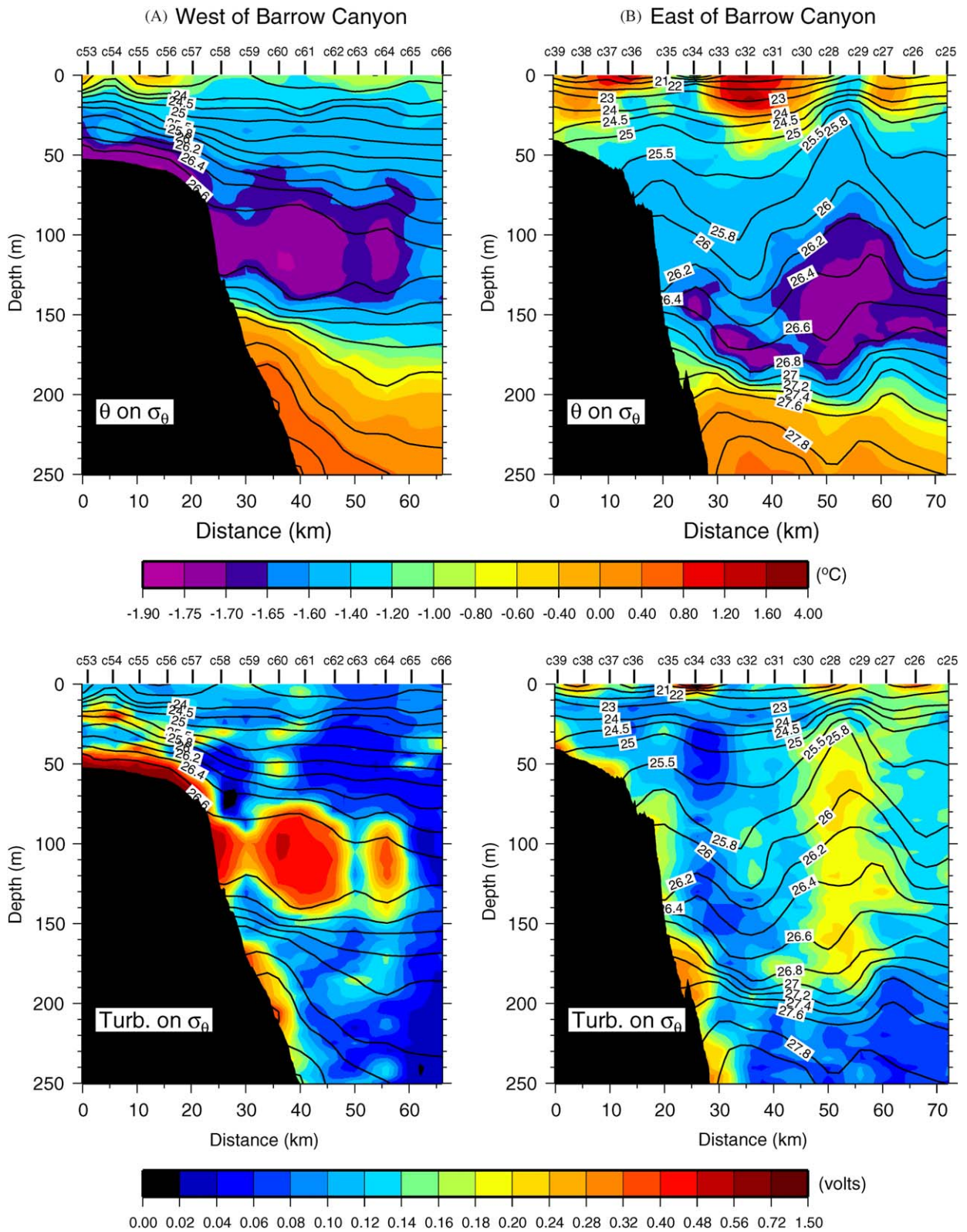[5] The 3-D structure of such a boundary current eddy was mapped out during the fall 2004 SBI cruise.

Fig. 12. Vertical sections of properties overlaid on potential density (kg/m³). The top panel shows potential temperature (color, °C); the bottom panel shows turbidity (color, volts). (A) Section 5, west of Barrow Canyon and (B) Section 3, east of Barrow Canyon.

Table 1
Properties of the anti-cyclonic, cold-core eddies

Eddy	σ_θ Layer (kg/m^3)	θ (°C)	Salinity	Turbidity (volts)	Fluorescence (µg/l)	Relative swirl speed (cm/s)	Rossby number
Section 3	26.4–26.75	−1.722	32.96	.194	.724	34	.28
Section 6	26.65–26.8	−1.735	33.23	.302	.076	9	.07
Section 5	26.65–26.8	−1.736	33.17	.432	.353	6	.05
Scicex 97	26.55–27.05	−1.778	33.37	—	—	25	.18

The potential temperature, salinity, turbidity, and fluorescence are values at the eddy core averaged over the density layer. The swirl speeds are computed using the dynamic-height distributions in Fig. 13B.

eddy that was spawned a few days earlier from the Alaskan Coastal Current exiting Barrow Canyon (G. Stossmeister, pers. Comm., 2003). Hence, this observation verifies the hypothesis of baroclinic instability put forth by Manley and Hunkins (1985), but it also casts doubt on their conjecture that these warm features evolve into subsurface pycnocline eddies, since the eddy is so light and is confined to such a shallow depth.

5.2.1. Regional differences

To compare the different cold-core eddies observed along the shelfedge, we computed cross-stream distributions of the different properties. In particular, for each eddy we identified the appropriate density range and computed layer averages across the feature. Results are presented in Table 1 and displayed in Fig. 13, revealing the anomalous nature of the eddies (for example, the low temperature core near −1.72 to −1.74 °C, Fig. 13A). The density of these features varies somewhat, but they are all in the salinity range of the upper halocline. This is consistent with the historical data analysis of Pickart (2004) who found that the boundary current consistently ventilated the upper halocline. As a measure of eddy strength, Fig. 13B shows the dynamic topography of the upper part of the eddy relative to its central pressure. One immediately sees that the eddy located to the east of Barrow Canyon is markedly stronger (and thicker) than the two eddies to the west (this is also true of the eddy at Section 2 farthest to the west, not shown). This is particularly evident in the computed Rossby numbers, which range from .3 to .05 (Table 1).

Is this east–west difference in eddy strength a regular pattern? Though we have only one realization east of Barrow Canyon, we suspect that it is. To consider this, we first demonstrate that the eastern
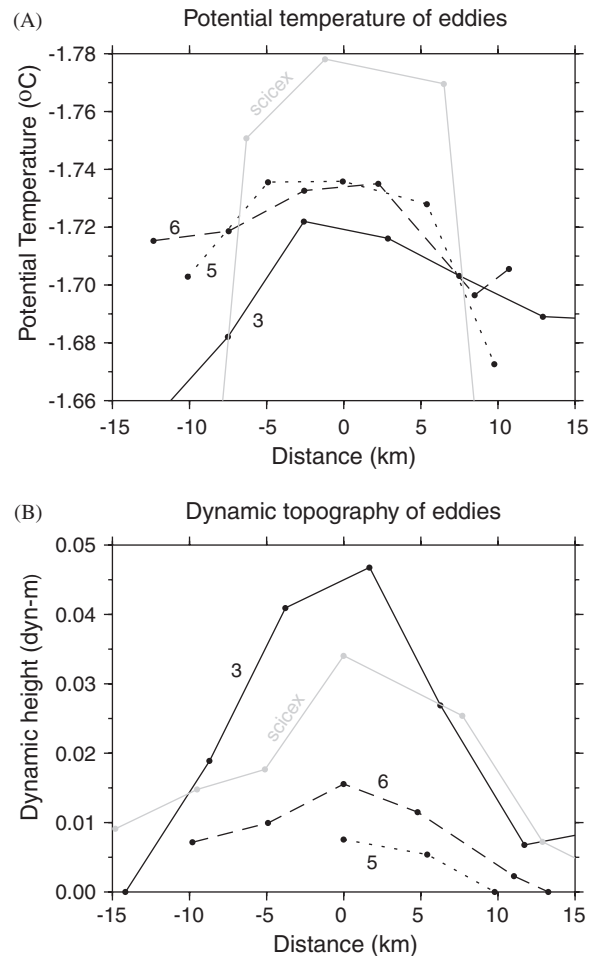

Fig. 13. Properties of the eddies observed on Sections 3,5 and 6 (black lines), as well as the Scicex Eddy (gray line). The features have been aligned horizontally at the origin of the abscissa. (A) Potential temperature (°C) averaged within the density layer of the eddy (see Table 1). (B) Dynamic height of the eddy relative to its central pressure: Section 3 (30 db relative to 140 db); Section 6 (50 db relative to 115 db); Section 5 (50 db relative to 115 db); Scicex 97 (60 db relative to 200 db). For Section 5, only the offshore side of the eddy is shown (since it is still pinching off).
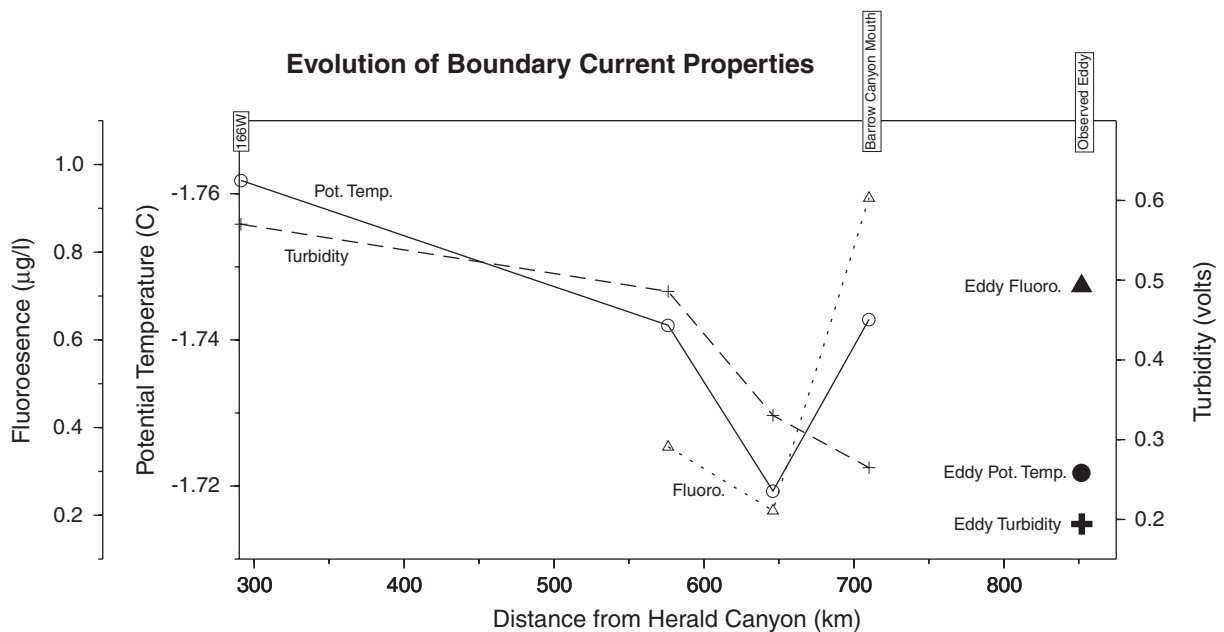
Evolution of Boundary Current Properties

Fig. 14. Downstream evolution of boundary current properties, averaged within the density layer $\sigma_\theta = 26.65-26.8$. Also shown are the properties at the core of the eastern eddy (see Table 1).

eddy originated from the dense water exiting Barrow Canyon, and not from the dense water exiting Herald Canyon from farther west. Fig. 14 shows the downstream evolution in properties of the boundary current from west to east, compared with those of the eddy east of Barrow Canyon. Note that all of the boundary current properties moderate as one progresses eastward from the Herald Canyon source (presumably from diffusion and eddy formation). This trend changes, however, at the mouth of Barrow Canyon where the current suddenly gets colder and higher in fluorescence (Fig. 14). This is consistent with the scenario described above whereby the reservoir of cold water at the head of Barrow Canyon feeds the current exiting the canyon—hence overpowering any dense water trying to enter the western end of the canyon from offshore. Recall that the high-fluorescence signal diffuses into the winter-transformed water at the head of Barrow Canyon (Fig. 5C); this is likely the source of the marked increase in fluorescence in Fig. 14. Essentially, the eastern eddy has values of temperature and fluorescence that are too extreme to have originated from the water west of the canyon (Fig. 14), but consistent with the water exiting through the canyon (after modification by mixing during the eddy-formation process).

Now consider the east–west differences in boundary current strength. We used the lowered-ADCP velocity data to reference the thermal wind shear in Section 5 (Fig. 12A) to quantify the eastward-flowing shelfbreak jet. Because the vertical structure of the lowered-ADCP velocity profiles agrees well with the geostrophic shear, this implies that tides are minimal at this location as in Barrow Canyon. The absolutely referenced boundary current core speed at this location (not shown) is 14 cm/s. By contrast, the winter-transformed water flows out of Barrow Canyon at speeds of up to 30 cm/s (keep in mind also that this velocity field has been smoothed, Fig. 3). This difference in current strength is consistent with the discrepancy in eddy swirl speeds observed on either side of the canyon (Table 1), implying that eddies formed from the Barrow Canyon outflow should be stronger than those originating from the Herald Canyon outflow.

5.2.2. Comparison to interior eddy

Muench et al. (2000) did a detailed survey of a cold-core, anti-cyclonic eddy in the interior of the Canada Basin, using data collected during the Scicex expedition in August 1997. The eddy was located roughly 175 km north of our easternmost hydrographic section (Fig. 1), and was similar in

character to the eddies found in our data set. Muench et al. (2000) argued that the Scicex Eddy likely originated from densified polynya water on the northeast Chukchi shelf (south of Barrow Canyon, see Cavalieri and Martin, 1994), and evolved into an eddy via the processes studied by Gawarkiewicz and Chapman (1995) and Chapman and Gawarkiewicz (1995). These authors demonstrated, in a numerical modeling framework, that dense water formed within a polynya is fluxed laterally away from the region of forcing by turbulent eddies. The eddies arise due to baroclinic instability of the frontal edge surrounding the polynya.

While this process may be happening on the shelf, such "polynya eddies" are probably not what Muench et al. (2000) observed in the middle of the Canada Basin. Gawarkiewicz (2000) extended the numerical modeling work to include shelfbreak topography, and showed that, in the absence of background flow, the polynya eddies tend to coalesce at the shelfedge and form a gravity current. Very little dense water is fluxed offshore, which led Gawarkiewicz (2000) to suggest that other mechanisms are necessary to transport the polynya water to the open basin. We argue that the Scicex Eddy was formed instead by instability of the shelfbreak jet in a similar manner to that observed in Fig. 12A. Furthermore, we suggest that the Scicex Eddy did not contain polynya water, but was filled with the more generic winter-transformed Bering water. The characteristics of the Scicex Eddy are included in Table 1 and displayed in Fig. 13. While it is colder and denser than any of the eddies we observed, this could be due to seasonal or interannual variability. (The temperature anomaly is greater because the Scicex Eddy was observed in mid-basin, surrounded by warmer water.) In terms of θ, S, and σ_θ the Scicex Eddy corresponds to Weingartner et al.'s (1998) intermediate winter mode water, not their cold hypersaline mode water (i.e. not the polynya water). Hence, like the eddies observed in our survey, the Scicex Eddy contains the generic wintertime water mass of the Chukchi Sea, and is of the correct density to ventilate the upper halocline of the Canada Basin.

Muench et al. (2000) also believed that the Scicex Eddy was over a year old, based in part on its calculated tritium–helium age. Fig. 13B shows that the eddy was in fact still quite strong. This suggests firstly that it was formed by the Barrow Canyon outflow, and secondly that it may not be very old.

Assuming that the winter-transformed Bering water is exiting the Chukchi Sea by early May of each year (consistent with the newly obtained mooring data), this gives a transit speed of 2.1 cm/s for the eddy if it were formed earlier that year (instead of the previous year, as suggested by Muench et al., 2000). One must also keep in mind that the tritium–helium age of a newly formed water mass often overestimates the true age. A particularly pertinent example of this is seen in Pickart et al. (1996), who sampled a newly formed subsurface anti-cyclone in the Labrador Sea, likely spawned by a similar instability process from the Labrador current (Pickart et al., 1997). The calculated tracer age was several years, whereas the eddy was formed only months earlier. Pickart et al. (1996) showed that this discrepancy arose because of incomplete atmospheric equilibration during the wintertime overturning of the water column. This same effect could be happening during the formation of the winter water in the Chukchi and Bering Seas.

6. Discussion

Our results demonstrate that the ubiquitous eddies of winter-transformed Bering water found throughout the Canada Basin are readily formed from the Chukchi/Beaufort shelfbreak current—likely from baroclinic instability. While the adjustment of the dense water through Barrow Canyon leads to a potential vorticity distribution which is conducive for such instability, we cannot say at this point how close to the mouth of the canyon eddies actually form. We can say, however, that eddies are spawned from both the Barrow Canyon outflow as well as the Herald Canyon outflow. The number of eddies we observed during our month-long hydrographic survey suggests that this process is an efficient, and perhaps even dominant, means of fluxing newly formed water offshore.

An obvious question to ask is, how many eddies would be required to ventilate the entire upper halocline of the Canada Basin? We estimate this as follows. Assuming that the average eddy is a right circular cylinder with radius = 10 km and thickness = 75 m, this gives a volume of 25 km^3 for a single eddy. The area of the Canada Basin is taken to be 10^6 km^2, and the thickness of the upper halocline to be 50 m. This means that the volume of winter-transformed Bering water in the Canada Basin is roughly 5×10^4 km^3. It is believed that the renewal time of the upper halocline is on the order

of 10 years (Aagaard et al., 1981; Carmack, 1990). If we assume 10–20 years, this gives an annual renewal rate of .08–.16 Sv. If we now assume that this renewal is due completely to eddies, it means that roughly 100–200 eddies are formed each year. How reasonable is this number? Based on historical observations of eddies from ice camps and drifting buoys, it is believed that at any one time the Canada Basin is filled with 100–200 such features (A. Plueddemann, pers. Comm., 2004). Hence, if an average eddy lifetime is on the order of a year, the estimated eddy population is consistent with our estimated formation rate. This calculation of course has significant uncertainties (as does the population estimate). For example, if the area of the Canada Basin and the thickness of the upper halocline are both increased by 20%, this implies a renewal rate of .11–.23 Sv, and hence 144–288 eddies formed per year. Also, we are assuming that all of the eddy volume is winter-transformed water (i.e. minimal entrainment from above or below).

What does this mean in terms of the fate of the Pacific water flowing through Bering Strait? In the mean, 0.8 Sv pass through the strait, but not all of this is winter-transformed water (or what will become winter-transformed water in the Chukchi Sea). As an upper estimate we assume that the winter water transport is 0.3 Sv (the synoptic value calculated above, which likely does not persist year round). This implies that somewhere between 30–75% of this water is fluxed offshore by eddies. What happens to the rest of the water? At least part of the shelfbreak jet is able to pass into the Canadian Arctic Archipelago (limited to about the upper 120–150 m of the water column). Using nitrate–phosphate ratios, Jones et al. (2003a, b) show that a high percentage of Pacific water is present in the major passages of the archipelago (Barrow Strait, Jones Sound, Nares Strait, and Smith Sound). In the salinity range of the upper halocline (approximately 33.0–33.5) the percentage of Pacific-origin water ranges from 60% to 100%.

Some of the winter-transformed Bering water also continues eastward along the edge of the Arctic into the Lincoln Sea north of Greenland. Hydrographic sections collected there during the early 1990s (Newton and Sotirin, 1997) reveal the presence of this water near the shelfedge. The structure of the boundary current reported by Newton and Sotirin (1997) is somewhat different than that found in our study (and also reported by Pickart, 2004). North of Greenland the strongest flow occurs in the Atlantic

layer, beneath the winter-transformed water. This, together with the relatively weak geostrophic shear seen by Newton and Sotirin (1997), seems to suggest that the majority of the Pacific-origin water passes into the archipelago. However, the shelfbreak in the Lincoln Sea is quite deep, and Newton and Sotirin's (1997) current meter array may have missed the majority of the Pacific water. Also, their hydrographic sections were occupied in April, too soon to see the seasonal presence of the winter-transformed Bering water.

A non-trivial amount of winter-transformed water almost certainly does pass through the Lincoln Sea and into Fram Strait, as evidenced by hydrographic surveys done in the strait. Jones et al. (2003c) measured a high percentage of Pacific-origin water using the nitrate–phosphate ratio technique. Taylor et al. (2003) reported similar findings using a different data set. Also, both papers presented vertical sections of silicate, clearly indicating the presence of winter-transformed Bering water in the same density range (i.e. upper halocline) as that reported here (Fig. 5A). Hence, while much of the winter-transformed water is seemingly fluxed into the interior Canada Basin by eddies, a significant fraction is transported directly out of the Arctic via the boundary current system, both through the Canadian Arctic Archipelago and through Fram Strait. The precise partitioning of the flux between these three different routes, however, remains to be sorted out.

Acknowledgments

References

Aagaard, K., 1984. The Beaufort Undercurrent. The Alaskan Beaufort Sea: Ecosystems and Environments. Academic Press, New york, pp. 47–71.

Aagaard, K., Roach, A.T., 1990. Arctic Ocean-shelf exchange: measurements in Barrow Canyon. Journal of Geophysical Research 95, 18,163–18,175.

Aagaard, K., Coachman, L.K., Carmack, E.C., 1981. On the halocline of the Arctic Ocean. Deep-Sea Research I 28, 529–545.

Borenas, K.M., Lundberg, P.A., 1988. On deep water flow through the Faroe Bank Channel. Journal of Geophysical Research 93, 1281–1292.

Bourke, R.H., Paquette, R.G., 1976. Atlantic water on the Chukchi Shelf. Geophysical Research Letters 3, 629–632.

Bush, A.B.G., McWilliams, J.C., Peltier, W.R., 1996. The formation of oceanic eddies in symmetric and asymmetric jets. Part II: late time evolution and coherent vortex formation. Journal of Physical Oceanography 26, 1825–1848.

Carmack, E.C., 1990. Large-scale physical oceanography of polar Oceans. In: Smith, Jr., W.O. (Ed.), Polar Oceanography, Part A: Physical Science. Academic Press, San Diego (406pp).

Cavalieri, D.J., Martin, S., 1994. The contribution of Alaskan, Siberian, and Canadian coastal polynyas to the cold halocline of the Arctic Ocean. Journal of Geophysical Research 99, 18,343–18,362.

Cenedese, C., Whitehead, J., 2000. Eddy formation at the shelfbreak. In: Proceedings of the shelf–basin interactions Pan-Arctic Meeting. SBI Project Office, 15–17.

Chao, S.-Y., Shaw, P.-T., 2003. Heton shedding from submarine-canyon plumes in an Arctic boundary current system: sensitivity to the undercurrent. Journal of Physical Oceanography 33, 2032–2044.

Chapman, D.C., 2000. The influence of an alongshelf current on the formation and offshore transport of dense water from a coastal polynya. Journal of Geophysical Research 105, 24,007–24,019.

Chapman, D.C., Gawarkiewicz, G.G., 1995. Offshore transport of dense shelf water in the presence of a submarine canyon. Journal of Geophysical Research 100, 13,373–13,387.

Coachman, L.K., Aagaard, K., Tripp, R.B., 1975. Bering Strait: The Regional Physical Oceanography. University of Washington Press, Seattle (172pp).

Danielson, S., 1996. The Chukchi Sea tides. M.Sc. Thesis, University of Alaska, Fairbanks, 51pp.

D'Asaro, E.A., 1988. Observations of small eddies in the Beaufort Sea. Journal of Geophysical Research 93, 6669–6684.

Furey, P.W., 1996. The large-scale surface wind field over the Western Arctic Ocean, 1981–1993. Masters Thesis, University of Alaska, Fairbanks, AK, 121pp.

Garrison, G.R., Becker, P., 1976. The Barrow submarine canyon: A drain for the Chukchi Sea. Journal of Geophysical Research 81, 4445–4453.

Garvine, R.W., Wong, K.C., Gawarkiewicz, G.G., McCarthy, R.K., Houghton, R.W., AikmanIII, F., 1988. The morphology of shelfbreak eddies. Journal of Geophysical Research 93, 15,593–15,607.

Gawarkiewicz, G.G., 2000. Effects of ambient stratification and shelfbreak topography on offshore transport of dense water on continental shelves. Journal of Geophysical Research 105, 3307–3324.

Gawarkiewicz, G.G., Chapman, D.C., 1995. A numerical study of dense water formation and transport on shallow, sloping continental shelves. Journal of Geophysical Research 100, 4489–4507.

Grebmeier, J.M., Harvey, R., 2005. The Western Arctic Shelf–Basin Interactions (SBI) project: an introduction. Deep-Sea Research II, this issue [doi:10.1016/j.dsr2.2005.10.004].

Hall, M.M., 1985. Horizontal and vertical structure of velocity, potential vorticity, and energy in the Gulf Stream. Ph.D. Thesis, Massachusetts Institute of Technology, 165pp.

Hall, M.M., 1994. Synthesizing the Gulf Stream thermal structure from XBT data. Journal of Physical Oceanography 24, 2278–2287.

Hill, V., Cota, G., 2005. Spatial patterns of primary production in the Chukchi Sea in the spring and summer of 2002. Deep-Sea Research II, this issue [doi:10.1016/j.dsr2.2005.10.001].

Johns, W.E., Watts, D.R., 1986. Time Scales and structure of topographic Rossby waves and meanders in the deep Gulf Stream. Journal of Marine Research 44, 267–290.

Jones, E.P., Swift, E.P., Anderson, L.G., Lipizer, M., Civitarese, G., Falkner, K.K., Kattner, G., McLaughlin, F., 2003a. Tracing Pacific water in the North Atlantic Ocean. Journal of Geophysical Research 108.

Jones, E. P., Rudels, B., Eert, A.J., Anderson, L.G., Azetsu-Scott, K., 2003b. Waters of Nares Strait in the Canadian Arctic Archipelago. In: Proceedings, ACSYS Final Science Conference, St. Petersburg, 11–14 November 2003.

Jones, E.P., Anderson, L.G., Jutterstrom, S., Swift, J.H., 2003c. Identifying sources of fresh water in the east greenland current. Eos Transactions, AGU 84 (46) Fall Meeting, Suppl., Abstract OS21C-1137.

Krishfield, R.A., Plueddemann, A.J., 2002. Eddys in the Arctic Ocean from IOEB ADCP data. Woods Hole Oceanographic Institution Technical Report WHOI-2002-09, 144pp.

Manley, T.O., Hunkins, K., 1985. Mesoscale eddies of the Arctic Ocean. Journal of Geophysical Research 90, 4911–4930.

Mountain, D.G., 1974. Bering Sea Water on the north Alaskan Shelf. Ph.D. Thesis, University of Washington, Seattle, WA, 153pp.

Mountain, D.G., Coachman, L.K., Aagaard, K., 1976. On the flow through Barrow Canyon. Journal of Physical Oceanography 6, 461–470.

Muench, R.D., Gunn, J.T., Whitledge, T.E., Schlosser, P., Smethie Jr., W., 2000. An Arctic Ocean cold core eddy. Journal of Geophysical Research 105, 23,997–24,006.

Munchow, A., Carmack, E.C., 1997. Synoptic flow and density observations near an Arctic shelfbreak. Journal of Physical Oceanography 27, 1402–1419.

Newton, J.L., Sotirin, B.J., 1997. Boundary undercurrent and water mass changes in the Lincoln Sea. Journal of Geophysical Research 102, 3393–3403.

Ou, H.W., Gordon, A.L., 1986. Spin-down of baroclinic eddies under sea ice. Journal of Geophysical Research 91, 7623–7630.

Paquette, R.G., Bourke, R.H., 1974. Observations on the coastal current of Arctic Alaska. Journal of Marine Research 32, 195–207.

Pedlosky, J., 1979. Geophysical Fluid Dynamics. Springer, New York (624pp).

Pickart, R.S., 2004. Shelfbreak circulation in the Alaskan Beaufort Sea: mean structure and variability. Journal of Geophysical Research 109.

Pickart, R.S., Smethie Jr., W.M., 1993. How does the deep Western Boundary Current cross the Gulf Stream? Journal of Physical Oceanography 23, 2602–2616.

Pickart, R.S., Smethie Jr., W.M., Lazier, J.R.N., Jones, E.P., Jenkins, W.J., 1996. Eddies of newly formed upper Labrador Sea water. Journal of Geophysical Research 101, 20,711–20,726.

Pickart, R.S., Spall, M.A., Lazier, J.R.N., 1997. Mid-depth ventilation in the Western Boundary Current system of the sub-polar gyre. Deep-Sea Research I 44, 1025–1054.

Plueddemann, A., Krishfield, R., Edwards, C., 1999. Eddies in the Beaufort Gyre, Ocean–Atmosphere–Ice Interactions (OAII) All Hands Meeting, 20–22 October, 1999, Virginia Beach, VA.

Pratt, L.J., Stern, M.E., 1986. Dynamics of potential vorticity fronts and eddy detachment. Journal of Physical Oceanography 16, 1101–1120.

Pratt, L.J., Deese, H.E., Murray, S.P., Johns, W., 2000. Continuous dynamical modes in straits having arbitrary cross sections, with applications to the Bab al Mandab. Journal of Physical Oceanography 30, 2525–2534.

Roach, A.T., Aagaard, K., Pease, C.H., Salo, S.A., Weingartner, T., Pavlov, V., Kulakov, M., 1995. Direct measurements of transport and water properties through the Bering Strait. Journal of Geophysical Research 100, 18,443–18,457.

Shaw, P.-T., Chao, S.-Y., 2003. Effects of a baroclinic current on a sinking dense water plume from a submarine canyon and heton shedding. Deep-Sea Research I 50, 357–370.

Signorini, S.R., Munchow, A., Haidvogel, D., 1997. Flow dynamics of a wide Arctic canyon. Journal of Geophysical Research 102, 18,661–18,680.

Spall, M.A., 1995. Frontogenesis, subduction, and cross-front exchange at upper ocean fronts. Journal of Geophysical Research 100, 2543–2557.

Taylor, J.R., Falkner, K.K., Schauer, U., Meredith, M., 2003. Quantitative considerations of dissolved barium as a tracer in the Arctic Ocean. Journal of Geophysical Research 108.

Weingartner, T.J., Cavalieri, D.J., Aagaard, K., Sasaki, Y., 1998. Circulation, dense water formation, and outflow on the northeast Chukchi shelf. Journal of Geophysical Research 103, 7647–7661.

Weingartner, T., Aagaard, K., Woodgate, R., Danielson, S., Sasaki, Y., Cavalieri, D., 2005. Circulation on the north central Chukchi Sea shelf. Deep-Sea Research II, this issue [doi:10.1016/j.dsr2.2005.10.015].

Winsor, P., Chapman, D.C., 2002. Distribution and interannual variability of dense water production from coastal polynyas on the Chukchi shelf. Journal of Geophysical Research 107.

Winsor, P., Chapman, D.C., 2004. Pathways of Pacific water across the Chukchi Sea: A numerical model study. Journal of Geophysical Research 109, C03002.

Woodgate, R.A., Aagaard, K., Weingartner, T.J., 2005. A year in the physical oceanography of the Chukchi Sea: Moored measurements from autumn 1990–1991. Deep-Sea Research II, this issue [doi:10.1016/j.dsr2.2005.10.016].